Characteristics of Biodegradable Poly(butylene succinate) Nanocomposites With Thermally Reduced Graphene Nanosheets

Pramoda Kumari Pallathadka,[1] Xue Qi Koh,[1] Akhila Khatta,[2] Gisha E. Luckachan,[3] Vikas Mittal[3]
[1]*Institute of Materials Research and Engineering, Materials Analysis and Characterisation Group, A*STAR (Agency for Science, Technology and Research), 4 Funsionopolis Way 117602, Singapore*

[2]*School of Materials Science and Engineering, Nanyang Technological University, 639798, Singapore*

[3]*Department of Chemical Engineering, The Petroleum Institute, Abu Dhabi, UAE*

Poly(butylene succinate) (PBS) is a biodegradable aliphatic polyester and is semicrystalline in nature. It has a wide range of engineering applications owing to its attractive combination of good processability and mechanical properties. PBS nanocomposites with graphene nanosheets were prepared by melt compounding. We report on their structure and their thermal, electrical, and mechanical properties. The thermal stability of the nanocomposite increased by 35°C compared with that of neat PBS. The crystallization and melting behavior of the PBS matrix in the presence of dispersed graphene nanosheets were studied by differential scanning calorimetry and polarised optical microscope. We also observed an interesting phenomenon in the PBS/graphene nanocomposites from our FTIR investigation. β-form of PBS crystals are formed in the composite samples with 5 wt% graphene loading, which otherwise forms in pure PBS only under stress. We observed ~12% modulus enhancement for 2 wt% PBS/graphene nanocomposites. The electrical conductivity increased to ~10^5-fold for 5 wt% PBS/graphene nanocomposites. POLYM. COMPOS., 38:E42–E48, 2017. © 2015 Society of Plastics Engineers

INTRODUCTION

Plastics have made a major contribution to our daily life but at the same time they have also posed serious environmental issues. Conservation and protection of the global environment has emerged as the main challenge in order to further improve the quality of life [1, 2]. In this light biodegradable polymeric materials may be seen as a promising alternative to non-degradable plastics. In fact the development of biodegradable polymeric materials with excellent properties has become an irreversible trend worldwide. Poly(butylene succinate) (PBS), a typical synthetic biodegradable aliphatic polyester, is generally synthesized from diols and dicarboxylic acids. It has potential applications as a packaging material that can alleviate environmental pollution caused by commodity polymers since it is not only biodegradable but also has a good elongation at break along with other physical properties similar to polyethylene. Among the industrially available biodegradable polymers, PBS is well known for its reasonable production cost and good performance characteristics [1–3]. However, it still lacks the mechanical and thermal properties required for industrial applications. Therefore, incorporating other suitable materials into the PBS matrix may be an effective way to enhance the utility of PBS.

Preparation and characterization of polymer nanocomposite materials have aroused a great deal of interest among researchers over the past few years. This is mainly due to their enhanced properties including mechanical strength, barrier behavior, thermal stability, and heat deflection temperature. This property enhancement is mainly due to the high aspect ratio and low density of the nanoparticle reinforcement in the polymer matrix [1–4]. Common nano-reinforcements are organoclay, carbon nanotubes (CNTs), graphite, polyhedral oligomeric silsesquioxanes, and SiO_2. Graphite has a layered structure similar to clay constituted by a large number of graphene nano-sheets held together by Van der Waals forces

Correspondence to: K.P. Pramoda; e-mail: pramoda-kp@imre.a-star.edu.sg or V. Mittal; e-mail: vmittal@pi.ac.ae
Contract grant sponsor: Agency for Science, Technology and Research (ASTAR); Contract grant sponsor: Institute of Materials Research and Engineering (IMRE), Agency for Science, Technology and Research (A*STAR), Singapore; The Petroleum Institute, Abu Dhabi, UAE.
Additional Supporting Information may be found in the online version of this article.
DOI 10.1002/pc.23824
Published online in Wiley Online Library (wileyonlinelibrary.com).

[5–11]. They form aggregates when dispersed in polymer matrix due to their poor miscibility with organic polymers; therefore pretreatment and modification of graphite is carried out to achieve a homogeneous dispersion of graphene nanosheets in the polymer matrix. The surface treatment of graphene makes it more compatible to the polymer matrix providing good dispersion, and resulting in composites with excellent mechanical and electrical properties [3–6].

There are a number of studies on PBS nanocomposites with fillers like TiO_2, silica, clay, carbon black, CNT but very limited studies with graphene or graphene oxide. Among biodegradable polymers, PBS has received an increasing amount of attention because of its biodegradability, abundant renewable source, and excellent processability [9–17]. However, their mechanical and thermal properties are often not sufficient to find as commercial and industrial applications. Findings from previous work [15–18] are persuasive that graphene is able to make polymeric materials much stronger and more protective. This study deals with the preparation of PBS/graphene nanosheets nanocomposites. Investigations of their detailed structure, morphology, thermal, electrical, and mechanical properties of the obtained PBS nanocomposites have been carried out to evaluate the influence of filler reinforcement on the properties of the neat PBS.

EXPERIMENTAL

Materials

PBS (Bionelle 1050 from Showa Highpolymer, Japan) was kindly donated by Prof. Shih from Chaoyang University, Taiwan. Thermally reduced graphene was produced by thermal exfoliation of precursor graphite oxide using modified Hummer's method. A short description for the preparation of graphene is as follows: 5 g of graphite powder was added with 125 mL concentrated H_2SO_4, to which 2.5 g of $NaNO_3$ was subsequently added. After stirring the mixture for 30 min while keeping in an ice-bath (5°C), 15 g of $KMnO_4$ was added and the temperature was raised gradually to 35°C. After stirring 2 h, deionized water was added and the temperature was raised to 100°C. Subsequently, the mixture was quenched and diluted by pouring it into 1.5 l deionized water. This was followed by addition of 30% H_2O_2 until the evolution of bubbles of hydrogen stopped. The solution was then filtered and the residues were dispersed in 2 l de-ionized water and were added with dilute HCl (6%) (2 l) to remove the SO_4^{2-} ions. The dispersion was filtered and the filtrate was analyzed for SO_4^{2-} and Cl^- ions using $BaSO_4$ and $AgNO_3$, respectively. The washed graphite oxide was dried under vacuum at 60°C for 24 h. Graphene was generated via thermal exfoliation of graphite oxide by placing 1 g in a long quartz tube with 25 mm internal diameter and sealed at one end. The sample was flushed with nitrogen, followed by insertion of the tube in a tube furnace preheated to 1,050°C. The tube was held in the furnace for 30 s. The conformation of graphene formation was achieved through Raman spectroscopy, microscopy, and X-ray diffraction.

Sample Preparation

Prior to the melt mixing process, the PBS resin was dried in a vacuum oven at 80°C overnight in order to remove any trace of moisture, which might cause its potential hydrolytic degradation during its melt processing. The PBS/graphene nanocomposites were then prepared using a corotating twin screw-extruder. The mixing temperature was kept around ~170°C at a screw speed of 270 rpm. Disk-shaped samples with a diameter of 25 mm and a thickness of 1 mm and rectangular samples were prepared using a hot press operated at 150°C and 10 kPa.

Characterizations

The nanocomposites were characterized for their structure, thermal, and mechanical properties. Several different tools were employed in their characterization. X-ray Diffraction (XRD) measurements were carried out in a Bruker GADDS powder X-ray diffractometer using a reflection geometry and CuKα radiation (Wavelength $\lambda = 0.154$ nm) operated at 40 kV and 40 mA. Differential scanning calorimeter was used to determine melting points and crystallization temperatures. Dielectric analyser (DEA) and dynamic mechanical analyser (DMA) were used to determine the glass transition temperatures of these nanocomposites. MicroXact 8 A4P-200 4-point probe resistivity mapping system, and nanoindentation measurements were performed to understand their conductivity and mechanical behavior. The effect of crystallization temperature on the crystalline morphology and spherullitic growth was studied via polarized optical microscopy (POM) coupled with a Linkam hot stage. The surface morphology was examined by transmission electron microscopy (TEM) using a JEOL 2000EX(II) (JEOL, Tokyo, Japan) on the microtomed samples. Thermal properties of the samples were analyzed using Netzsch thermogravimetric analyzer (TGA). Nitrogen was used as a carrier gas and the scans were obtained from 50°C to 700°C at a heating rate of 20°C/min.

FTIR-ATR measurements were conducted on PBS and PBS/graphene nanocomposites using a Bruker VERTEX 70 spectrometer equipped with a Pike MIRacle ZnSe ATR accessory, DT-DLaTGS detector and KBr beamsplitter. ATR accessory had a ZnSe crystal of refractive index 2.4@1,000 cm^{-1} with a depth penetration of 2 mm at 45° angle of incidence. IR acquisitions between 4,000 and 600 cm^{-1} were made using the software OPUS at 4 cm^{-1} resolution with an average of 60 scans. Normal ATR spectra of PBS were obtained by keeping a square piece of PBS on the ZnSe crystal surface. Stressed PBS spectra were collected by smashing the square piece by applying higher mechanical stress using the piston in ATR accessory.

RESULTS AND DISCUSSION

Structure of the Neat PBS and PBS/Graphene Nanocomposites

XRD is an important tool for determining the crystal structure of the polymer in the nanocomposites. XRD analysis was performed at room temperature, and the patterns are shown in Fig. 1a. The diffraction patterns of the neat PBS and its graphene nanocomposite samples are quite similar. This indicates that the samples had the same crystal structure. The main characteristic diffraction peaks observed at 2θ values of 19.7, 21.9, and 22.8° were assigned to (020), (021), and (110) planes. In the case of nanocomposites, the diffraction peaks more or less were unchanged from neat PBS indicating that the incorporation of graphene nanosheets in the PBS matrix did not alter the crystal forms. A similar observation was made by Liang et al in carbon fiber reinforced PBS composites [19]. Additional insights into the crystal forms gained from the FTIR-ATR spectra of pure PBS and its nanocomposites are presented in Fig. 1b and c. Pure PBS exhibited a different spectrum on application of mechanical stress (as shown in Fig. 1b) compared with the normal PBS spectrum. ATR spectrum of PBS collected at normal conditions (Fig. 1b) showed ester C═O stretching vibrations at 1,714 cm^{-1}, CH_2 bending at 1,470 and 1,414 cm^{-1} as well as CH_2 wagging at 1,375 and 1,360 cm^{-1}. Multiple bands in the regions of 1,300–1,210 cm^{-1} and 1,200–1,100 cm^{-1} were attributed, respectively, to asymmetric and symmetric stretching vibrations of C—O—C linkage. O—C—C stretching vibrations were observed at 1,044 cm^{-1} and the region below 1,000 cm^{-1} corresponded to CH_2 sketch deformations [20–23]. Application of a mechanical stress significantly decreased the intensity of C—O—C asymmetric vibrations and the peak maxima of symmetric vibration shifted from 1,173 to 1,153 cm^{-1} (Fig. 1b). A doublet corresponding to CH_2 twisting appeared at 1330–1310 cm^{-1} [24]. Changes in the intensity and peak shift of CH_2 bending and wagging vibrations were also observed. Since IR is sensitive to conformational changes of polymer chains, it can be deduced from the ATR results that PBS polymer chains underwent phase transitions with the applied stress. Ichikawa et al. reported two crystalline modifications PBS: α- and β- forms [25, 26]. The authors observed α-form in the original fiber and β-form in a strained fiber. The solid-state crystal transitions between α- and β-forms were reversible with respect to the successive application and release of strain. Therefore, the spectra obtained under stress and normal conditions in Fig. 1b can be assigned, respectively, to β- and α-forms of PBS polymer. It is clear from Fig. 1b that the shift and intensity changes of the IR bands in the region from 1400 to 1100 cm^{-1} are highly sensitive to the α-β phase transitions. Considering that the bands at this region are strongly correlated to the C—O—C stretching modes

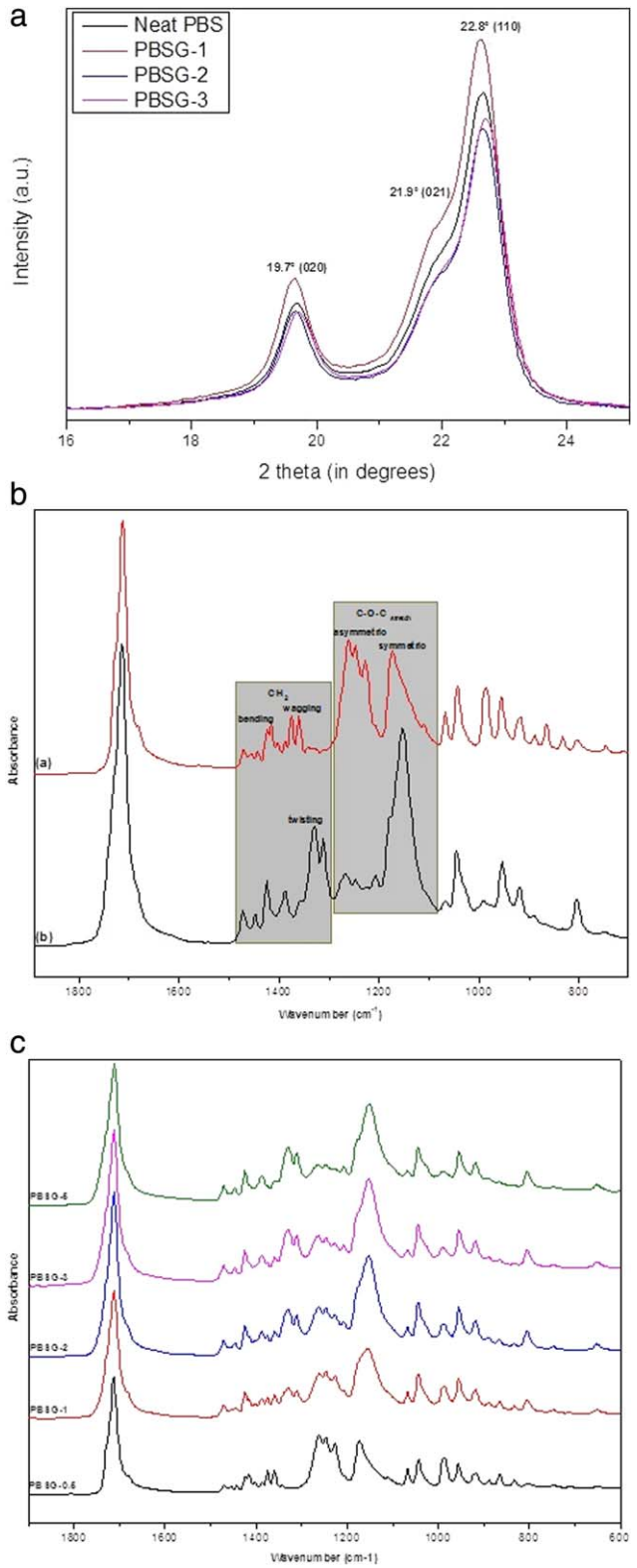

FIG. 1. (a) XRD patterns of neat PBS and PBS/graphene nanocomposites. (b) FTIR-ATR spectra of PBS taken under normal and stressed conditions; (c) FTIR-ATR spectra of PBS/graphene nanocomposites with different percentages of graphene taken under normal conditions.

DOI 10.1002/pc

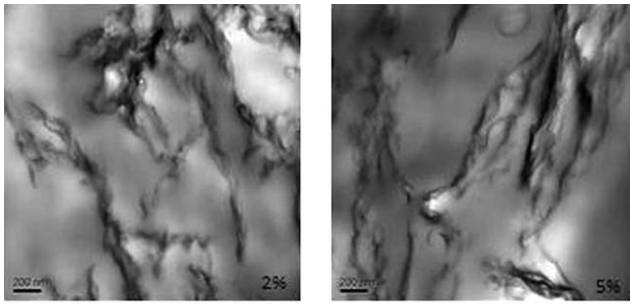

FIG. 2. TEM morphology of PBS/graphene nanocomposites (a) 2 and (b) 5 wt%.

resulting from different intermolecular interactions of ester groups, the relatively large peak shift and intensity change indicated that there were intense twists in the segments of C—O—C linkages during the α-β transition process of PBS [25, 26]. Furthermore, the changes in the intensity of CH_2 bending and wagging mode and formation of new CH_2 twisting vibrations undoubtedly demonstrate a cooperative response of all PBS chain segments during the transition process [25, 26]. All spectra of PBS/G nanocomposites given in Fig. 1c were collected under normal conditions. IR spectra similar to α form of PBS was observed at a low percentage of 0.5% filler content. On further increase of graphene to 1%, new CH_2 twisting bands started to appear at 1330–1310 cm^{-1} followed by an intensity decrease of C—O—C asymmetric stretching at 1300–1210 cm^{-1} and the peak maxima shift of C—O—C symmetric stretching from 1172–1153 cm^{-1}. These changes became more prominent at higher graphene concentrations in the nanocomposites and finally a spectrum similar to β- form of PBS was observed for PBS/5 wt% graphene loaded nanocomposite. It should be noted that β- form of PBS is unstable and is formed only under stressed conditions [27]. Gradual observation of this form in the nanocomposites under normal conditions as a function of graphene content indicated that the graphene platelets incorporated in the polymer matrix stabilized PBS in its β- form during the synthesis process. To reveal the dispersion state of graphene in the PBS matrix, TEM was used to observe a section of PBS/graphene nanocomposites as shown in Fig. 2a and b. TEM images confirm that the graphene nanosheets were homogeneously dispersed in the PBS matrix.

Thermal Properties of PBS/Graphene Nanocomposites

TGA curves (as shown in Supporting Information Fig. S1) of PBS and PBS/graphene nanocomposites under nitrogen atmosphere and their 5% weight loss temperatures are tabulated in Table 1. The 5% weight loss temperature for neat PBS is around 320°C and it progressively increases to 355°C at 5 wt% graphene loading. This means that the T_d of the nanocomposite

TABLE 1. Thermal properties of PBS/graphene nanocomposites.

Sample	T_d (°C)	T_m (°C)	Delta H (J/g)	% Crystallinity
PBS	320	110.9	79.8	39.9
PBS/GNC0.5	330	111.0	64.3	32.5
PBS/GNC1	342	111.1	63.4	31.7
PBS/GNC2	347	111.1	62.6	31.3
PBS/GNC3	354	111.1	62.2	31.1
PBS/GNC5	355	111.2	61.3	30.7

increased by 35°C compared with that of the pristine PBS sample indicating that the layered structure of graphene improves the thermal stability of the PBS matrix. It is clear that the incorporation of thermally reduced graphene nanosheets into the PBS matrix enhances its thermal degradation temperature. The enhanced thermal stabilization may be ascribed to a good dispersion of graphene nanosheets in the PBS matrix. A well dispersed nanosheet would form an effective barrier to volatile molecules produced during the PBS thermal decomposition. A similar result was obtained for other filler reinforced PBS nanocomposites [19, 28].

Differential scanning calorimetry (DSC) experiments on neat PBS and its graphene nanocomposite samples were carried out to understand the effect of incorporating graphene nanosheets on the crystallization behavior of the PBS matrix. Figure 3 shows the DSC cooling thermograms for neat PBS and its nanocomposites measured at a cooling rate of 10°C/min. The exothermic peak representing the crystallization peak temperature of PBS (73°C) increases with the incorporation of graphene nanosheets (77°C) implying that the crystallization of PBS is faster in the presence of graphene nanosheets. The graphene loadings have heterogeneous nucleation effects on the crystallization of PBS. It is believed that the addition of graphene nanosheets induces the crystallization of PBS.

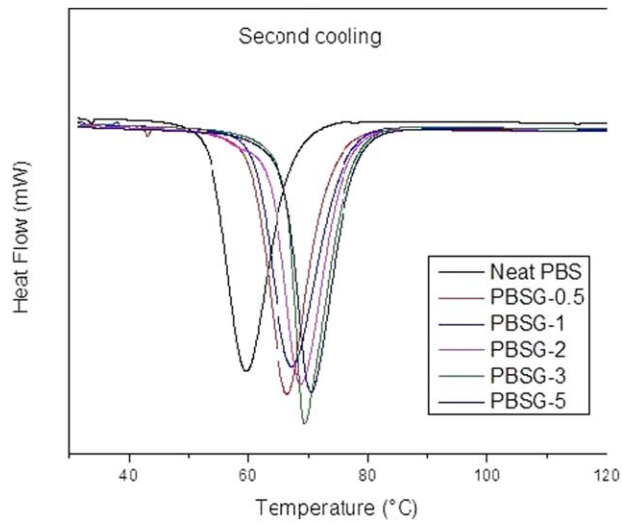

FIG. 3. DSC cooling thermogram for Neat PBS and its graphene nanocomposites.

TABLE 2. Electrical conductivity of PBS/graphene nanocomposites.

Sample	Sheet resistance	Thickness (cm)	Resistivity	Conductivity (S/cm)
PBS	2.01E + 09	0.15	0.302	3.32 E-09
PBS/GNC1	1.38E + 09	0.14	0.194	5.16 E-09
PBS/GNC2	1.37E + 09	0.15	0.206	4.85 E-09
PBS/GNC5	3.25E + 03	0.15	0.488	2.05 E-03

The values are averaged from 6 trials.

However, compared with neat PBS, the T_m (~111°C) is not much affected by the addition of the graphene nanosheets (as shown in Supporting Information Fig. S2), probably due to their small size and the low content of the graphene nanosheets in the nanocomposites. In addition, both the melting and crystallization peaks in PBS/graphene nanocomposites are narrower than in neat PBS suggesting a narrower crystallite size distribution in PBS/graphene nanocomposites.

The crystallinity (χ_c) in all samples is calculated as follows:

$$\chi_c(\%) = \frac{\Delta H_m}{\Delta H_0} \times 100\%$$

where ΔH_m is the measured melting enthalpy (from DSC) and ΔH_o is the enthalpy of pure PBS crystal (200 J/g) [29]. As shown in Table 2, the crystallinity of PBS/graphene nanocomposites is reduced after adding the graphene. However, the change in PBS crystallinity is too small to induce any significant impact on the mechanical properties of the composites. Therefore, the significant reinforcement of the strength and modulus for PBS/graphene nanocomposites can be largely attributed to the homogeneous dispersion of graphene sheets in the polymer matrix and the strong interfacial interactions between both components [30].

The nucleation effect of the nanofillers and the spherulite evolution during the melt crystallization for the neat PBS and its nanocomposites were monitored with the help of POM. The samples were heated above their melting points, and cooled to their peak crystallization temperature, as determined previously from DSC. Micrographs were taken of their crystal morphology and the time taken for full crystallization within the field of view was recorded (Fig. 4). The spherulites that were formed in neat PBS (Fig. 4a) were regular and around 50 μm in size, which is typical for homogenous crystallization. However, the spherulites of the PBS/graphene nanocomposites are randomly spread out and not uniform in size, as the fillers act as nucleating sites for heterogeneous nucleated crystallization. In addition, in agreement with the DSC data, crystallization takes place within a shorter time as compared with neat PBS. It supports the fact that the graphene nanosheets dispersed in the nanocomposites served as nucleating agents for PBS crystals during their melt crystallization.

Electrical Properties of PBS/Graphene Nanocomposites

Table 2 represents the surface electrical conductivity of PBS/graphene nanocomposites. Their electrical conductivity increases gradually with increasing loading of the graphene nanosheets. The electrical conductivity increased from 3.32×10^{-9} S/cm for neat PBS to 2.05×10^{-3} S/cm for 5 wt% PBS/graphene nanocomposite clearly indicating a 10^5-fold. This improvement can be attributed to the formation of interconnected conducting networks formed by graphene nanosheets in the PBS matrix. Binti et al. showed that the electrical conductivity of PBS/CNT composites increased with the addition of CNT content [31].

In many real time applications, a polymer nanocomposite will be subjected to different temperature and frequencies. DEA can provide reliable information over the relaxation behavior of these composites. In order to evaluate the effect of graphene nanosheets on temperature dependent relaxation behavior of PBS matrix, their thermo-mechanical properties were measured from −100 to 100°C and are plotted in Fig. 5a–c. The glass transition temperature (T_g) of the nanocomposites shifted to a higher temperature with the increase of the graphene content: the T_g values were ~2°C to ~20°C at the graphene nanosheets loading of 0, 1, and 2 wt%, respectively. The increase in T_g with addition of graphene nanosheets is nearly 18°C and correlated to the restricted movements of the PBS polymer chains due to their interaction with the graphene nanosheets. Figure 5a shows the variation in permitivity with temperature at 100 kHz. Inside the tested temperature range, graphene-reinforced nanocomposites show substantially higher values of permittivity from 3.2 to 4.2 compared with neat PBS (2.4 to 2.7). The increase in their permittivity upto 10°C can be attributed to the immobilization of polymer chains onto the graphene surface increasing the effective volume of the filler.

Dynamic Mechanical Properties of PBS/Graphene Nanocomposites

Figure 6 shows the storage modulus (G'), and tan δ plots with temperature for neat PBS and PBS/graphene nanocomposites. G' is related to the ability of material to

FIG. 4. POM morphology of (a) Neat PBS and (b) PBS-1 wt% Graphene nanocomposites.

DOI 10.1002/pc

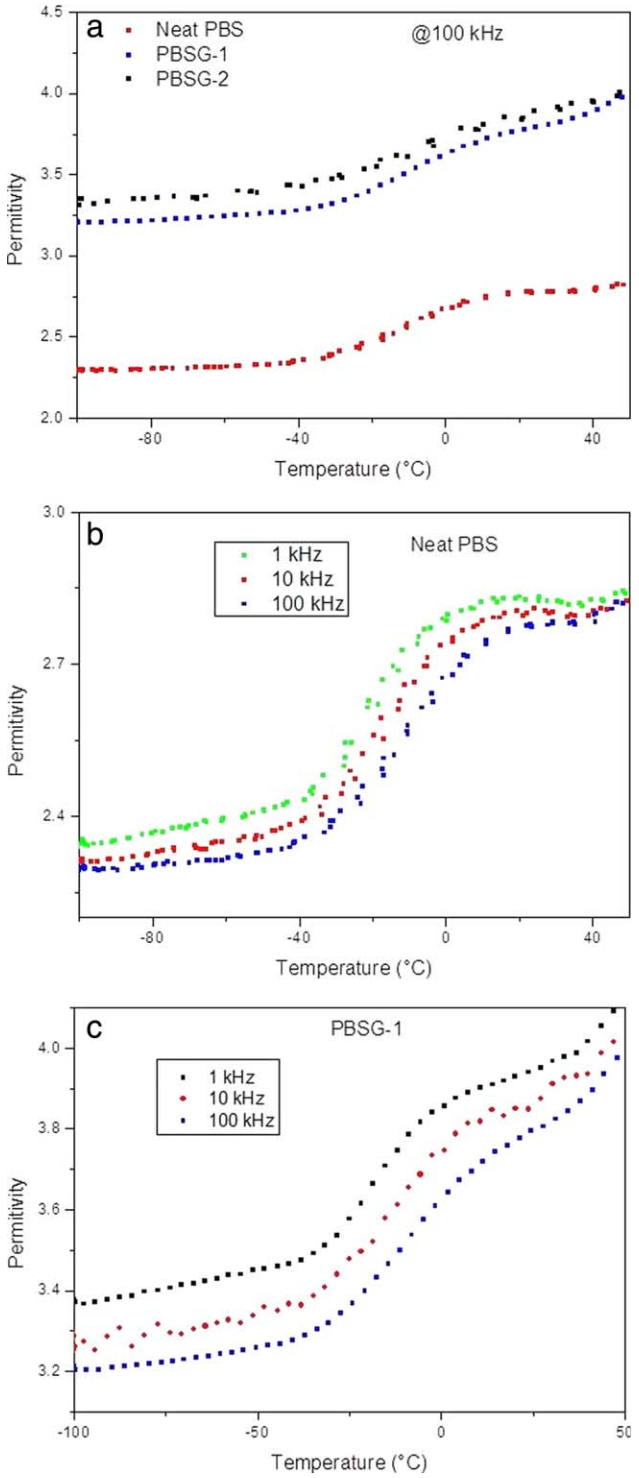

FIG. 5. (a) Permitivity (e') versus temperature for Neat PBS and its nanocomposites. (b) Permitivity (e') versus temperature for Neat PBS as a function of frequency. (c) Permitivity (e') versus temperature for PBS/graphene nanocomposites as a function of frequency.

store energy when an oscillatory force is applied, and tangent delta is related to the dampening ability of the composites. As shown in Fig. 6, the storage modulus of PBS/graphene nanocomposites exhibit negligible increase with small increases in graphene nanosheets loading up to the

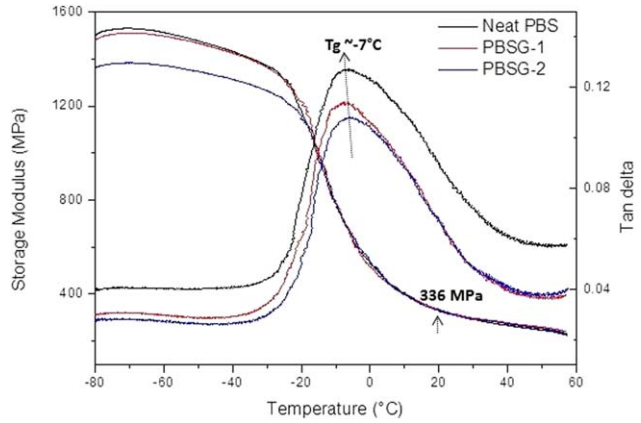

FIG. 6. Storage modulus (G'), and tan δ plots with temperature for Neat PBS and its nanocomposites.

glass transition temperature range. Beyond this the modulus of the nanocomposites is close to that of neat PBS. This implies that graphene nanosheets could enhance the rigidity of the nanocomposites due to their high surface area and good miscibility in the PBS matrix. The glass-transition temperature (T_g) is usually determined by the tan δ peak temperature in DMA. As shown in Fig. 6, the T_g of $\sim$7°C for both the neat PBS and for the nanocomposites indicates that the movements of the PBS polymer chains are restricted to a certain degree because of their grafting to the graphene nanosheets.

Nanoindentation tests were performed to measure the modulus and hardness of the PBS/graphene nanocomposites (Table 3). The values are averaged across 12 indents ranging over indentation depths of 1,200–1,500 nm. Typical load-displacement curves for the neat PBS and its GNS nanocomposites are shown in Supporting Information Fig. S3. The incorporation of graphene nanosheets in the nanocomposites improves the modulus and hardness of PBS matrix. There is a slight increment in the mechanical properties of the PBS/graphene nanocomposite compared to neat PBS. The presence of graphene nanosheets dispersed homogeneously in the PBS matrix are likely responsible for the improved thermal and mechanical properties of the polymer nanocomposites in this study.

CONCLUSIONS

PBS based nanocomposites with graphene nanosheets as nanofillers were prepared by melt mixing. As shown in

TABLE 3. Modulus and hardness measurement using nanoindentation.

Sample	Modulus (GPa)	Hardness (GPa)
PBS	1.15 ± 0.39	0.07 ± 0.02
PBS/GNC1	1.02 ± 0.23	0.08 ± 0.02
PBS/GNC2	1.32 ± 0.26	0.09 ± 0.03

The values are averaged on indentation depth of 1,200–1,500 nm from 12 indents.

the TEM images of the nanocomposites, it was confirmed that the graphene nanosheets were well dispersed in the PBS matrix. The XRD results showed that the addition of graphene nanosheets had almost no effect on the crystal structure. However, FTIR reveals that the β-form of PBS crystal was formed in the composites and was especially significant at 5 wt% graphene loading. The thermal stability of PBS/graphene composites is nearly 35°C higher than those of neat PBS. The thermal, electrical, and mechanical behavior of the nanocomposites with 1 wt% graphene nanosheets showed an improvement over the original PBS matrix. These enhancements could be due to a homogeneous dispersion of the graphene nanofillers in the matrix. Our POM and DSC studies have shown that the graphene loadings have heterogeneous nucleation effects on the crystallization of PBS.

ACKNOWLEDGMENTS

Contract grant sponsor: Institute of Materials Research and Engineering (IMRE), Agency for Science, Technology and Research (A*STAR), Singapore; The Petroleum Institute, Abu Dhabi, UAE.

REFERENCES

1. R. Krishnamoorti and A.V. Richard, Eds., *Polymer Nanocomposites: Synthesis, Characterization and Modelling*, American Chemical Society (2002).
2. P.M. Ajayan, L.S. Schadler, and P.V. Braun, *Nanocomposite Science and Technology*, Wiley-vcH verlag GmbH & Co KGaA, Weinheim (2003).
3. D. Bikiaris, *Polym. Degrad. Stab*., **98**, 1908 (2013).
4. S.S. Ray, S. Vaudreuil, A. Maazouz, and M. Bousmina, *J. Nanosci. Nanotechnol*., **6**, 2191 (2006).
5. K.P. Pramoda, N.T.T. Linh, C. Zhang, and T.X. Liu, *J. Appl. Polym. Sci*., **111**, 2938 (2009).
6. Y. Xu, W. Hong, H. Bai, C. Li, and G. Shi, *Carbon*, **47**, 3538 (2009).
7. T. Miyata and T. Masuko, *Polymer*, **39**, 1399 (1998).
8. G.Z. Papageorgiou and D. Bikiaris, *Polymer*, **46**, 12081 (2005).
9. S.S. Ray, K. Okamoto, and M. Okamoto, *Macromolecules*, **36**, 2355 (2003).
10. Y.F. Shih, *J. Polym. Sci. Part B Polym. Phys*., **47**, 1231 (2009).
11. G.Z. Papageorgiou, D.S. Achilias, and D. Bikiaris, *Macromol. Chem. Phys*., **208**, 1250 (2007).
12. J. Huang, X. Lu, N. Zhang, L. Yang, M. Yan, H. Lin, and G. Zhang, *Polym. Compos*., **35**, 53 (2014).
13. M. Snowdon, A.K. Mohanty, and M. Misra, *Macromol. Mater. Eng*., **300**, 118 (2015).
14. X. Wang, H. Yang, L. Song, Y. Hu, W. Xing, and H. Lu, *Compos. Sci. Technol*., **72**, 1 (2011).
15. S.I. Han, J.S. Lim, D.K. Kim, M.N. Kim, and S.S. Im, *Polym. Degrad. Stab*., **93**, 889 (2008).
16. J. Bian, L. Han, X. Wang, X. Wen, C. Han, S. Wang, and L. Dong, *J. Appl. Polym. Sci*., **116**, 902 (2010).
17. A.A. Vassiliou, D. Bikiaris, K. El Mabrouk, and M. Kontopoulou, *J. Appl. Polym. Sci*., **119**, 2010 (2011).
18. X.W. Wang, C.A. Zhang, P.L. Wang, J. Zhao, W. Zhang, J.H. Ji, K. Hua, J. Zhou, X.B. Yang, and X.P. Li, *Langmuir*, **28**, 7091 (2012).
19. J. Liang, C. Ding, Z. Wei, L. Sang, P. Song, G. Chen, Y. Chang, J. Xu, and W. Zhang, *Polym. Compos*., **36**, 1335 (2015).
20. X. Wang, L. Song, H. Yang, H. Lu, and Y. Hu, *Ind. Eng. Chem. Res*., **50**, 5376 (2011).
21. C. Yan, Y. Zhang, Y. Hu, Y. Ozaki, D. Shen, Z. Gan, S. Yan, and I. Takahashi, *J. Phys. Chem. B*, **112**, 3311 (2008).
22. Y.J. Phua, W.S. Chow, and Z.A. Mohd Ishak, *Express Polym. Lett*., **7**, 340 (2013).
23. H.S. Kim, H.J. Kim, J.W. Lee, and I.G. Choi, *Polym. Degrad. Stab*., **91**, 1117 (2006).
24. G. Socrates, Eds., *Infrared and Raman Characteristics Group Frequencies*, 3rd ed. Wiley, Chichester, New York (1994).
25. Y. Ichikawa, J. Suzuki, J. Washiyama, Y. Moteki, K. Noguchi, and K. Okuyama, *Polymer*, **35**, 3338 (1994).
26. Y. Ichikawa, H. Kondo, Y. Igarashi, K. Noguchi, K. Okuyama, and J. Washiyama, *Polymer*, **41**, 4719 (2000).
27. E. Adamopoulou, "Poly(butylene succinate): A promising biopolymer," PhD Thesis University of Piraeus, Greece (2012).
28. D. Bikiaris, *Thermochim. Acta*, **523**, 25 (2011).
29. X. Wang, J. Zhou, and L. Li, *Eur. Polym*., **43**, 3163 (2007).
30. M.K. Hong, S.W. Ko, J.H. Park, H.J. Choi, and J.H. Kim, *J. Nanosci. Nanotechnol*., **11**, 5352 (2011).
31. A.F. Binti and M. Raja, *Polym. Compos*., **31**, 1309 (2010).